The Effects of Nano In_2O_3 and ZnO on the CO Gas Detection of the SnO_2 Sensor

B. Hashemi[1], R. Atazadegan[1]

Abstract

The pellet-type SnO_2 sensor was synthesized by the solid state method and the effects of additives such as nano ZnO (1-12 mol %) and nano In_2O_3 (1-10 mol %) on the CO gas sensitivity of sensor were investigated. The optimum sintering temperature was chosen 800°C because of the porosity content of the samples. The phase analysis and microstructure of the samples were studied by x-ray diffraction and scanning electron microscopy, respectively. Results show that the electrical resistivity variations of the samples with time increased by increasing the amount of additives up to the optimum value for each additive. These optimum values were 10 and 7.5mol% for nano ZnO and nano In_2O_3, respectively. The best sensitivity and recovery and response times were obtained in the co-doped sample containing 10 mol% nano ZnO and 7.5 mol% nano In_2O_3. The higher values of the additives decreased the sensitivity of the samples due to the formation of undesirable phases.

Keywords: SnO_2 Sensor; ZnO; In_2O_3; CO Gas; Resistivity

1. Introduction

The N-type semiconductor gas sensors based on SnO_2 have been used for the detection of CO gas due to the low cost of the fabrication and simple sensing method. CO is a colorless, tasteless, widespread and toxic gas, which can have negative effects on human health even at low concentrations. In air, oxygen is chemisorbed to the surface of SnO_2 and depletes electrons from it, leading to the reduction of conductivity. When SnO_2 is exposed to the CO gas, the chemisorbed oxygen reacts with gas and electrons are reintroduced into the conduction band, resulting in an increase in conductivity [1].

A gas sensor should have high sensitivity, quick response-recovery, low operating temperature, gas selectivity and long stability. Hence, in recent years, noble metals or metal oxides have been added to SnO_2 sensors to achieve these characteristics [2-8]. The sensor properties are also dependent on the fabrication process. It affects the microstructure and crystal size of the sensor as well as the oxygen absorption properties of the sensor [9-13].

In the composite-type sensors, utilizing the mixture between semiconductor oxides, such as ZnO and SnO_2 or In_2O_3 and SnO_2 enhances the sensitivity due to the heterogeneous interfaces [5, 14-17]. However, when a composite sensor is synthesized by the solid state or conventional method, the average size of additives determines the optimum value of each additive. As to these values, the structural and phase changes are minimum and the sensor has the best sensing properties. In this study, different amounts of nano ZnO and In_2O_3 were added to the pellet form SnO_2 samples as additives to investigate their effects on the gas sensing properties of SnO_2. The gas sensitivity and electrical resistivity of the samples were explained according to the cations replacement and phase composition of the samples.

2. Experimental

For the preparation of the samples by the solid state method, nano powders (nano zinc oxide (Merck, 98.9%) and nano indium oxide (Merck, 99.9%)) were dispersed in the isoperapanol/Polyvinylpyrrolidone (PVP) solution and then appropriate amounts of tin

1- Department of Materials Science and Engineering, School of Engineering, Shiraz University, Shiraz, Iran.

Corresponding author: B. Hashemi, Department of Materials Science and Engineering, School of Engineering, Shiraz University, Shiraz, Iran. Email: hashemib@shirazu.ac.ir

oxide powder (Merck, 99.1%) and additives were ball-milled with zirconia balls in ethanol with a ball to the powder ratio of 20:1 for 24h. The rotation speed was 100 rpm. After drying, the mixture was pressed by a pressure of 200 MPa into pellets with a diameter of 10 mm and a thickness of 2 mm. The samples were sintered at 800˚C for 3 h in air. The heating rate was 5°C/min and then the samples were furnace cooled. Sintering at higher temperatures produced undesirable phases and decreased the porosity content of the samples.

X-ray diffraction (XRD) (Brucker D8-Advance with CuKα radiation) was used for the phase analysis of the samples. The density of the samples was determined by the Archimedes method (ASTM-C20). The grain size and morphology of the sintered samples were examined by scanning electron microscopy (SEM, Leica Cambridge, Stereoscan S 360).

For the measurement of electrical resistivity, the flat surface of the samples were polished and coated with Ag paste for the electrode. Then the samples were heated at 250 °C for 30 min in order to remove the absorbed moisture. After that the samples were placed in a quartz vacuum chamber to measure the electrical resistivity changes and CO gas sensing properties. The resistance value in air and its variation with time in 200 ppm CO were measured sequentially. The flow rate of gases was controlled using a mass flow controller and the relative gas humidity was constant in the chamber. The sensor sensitivity (S) was defined as the ratio of the samples resistance in dry air (R_a) to that in the presence of CO gas (R_g). The time taken by the samples to achieve 90% of the total resistance change was defined as the response time in the case of adsorption or the recovery time in the case of desorption.

3. Result and Discussion

The microstructures of the undoped SnO_2 and doped samples with 10mol% ZnO, 7.5 mol% In_2O_3 and 10 mol% ZnO-7.5 mol% In_2O_3 are shown in Fig. 1. As seen, no appreciable differences exist in the microstructure, and particle sizes are almost the same. Therefore, the additives do not have considerable effects on the microstructures and the change in the sensor properties is due to other effects.

Fig. 2 shows the XRD patterns of pure SnO_2 and doped samples with different amounts (mol %) of nano ZnO. The peaks correspond to the rutile structure of SnO_2. In the doped samples, a shift to higher 2θ values is seen in the diffraction peak positions and a new peak is observed in the sample with 7 mol% ZnO. This can be explained according to the ionic radius of Sn^{+4} and Zn^{+2}. When ZnO is added to the SnO_2, Zn^{+2} replaces Sn^{+4}. Because the ionic radius of Zn^{+2} (74 pm) is

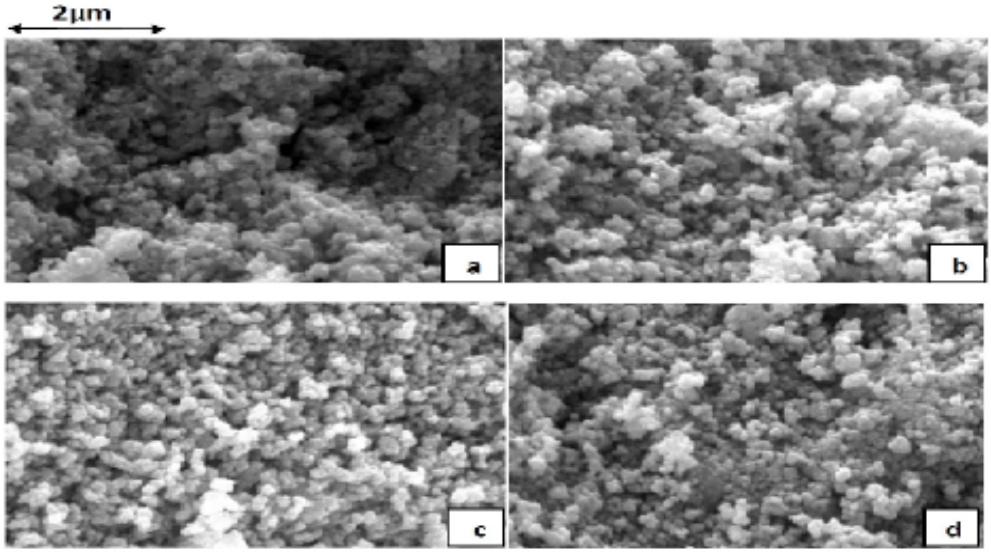

Fig. 1. SEM micrograghs of fractured surface of (a) undoped SnO_2 and doped SnO_2 samples with (b) 10mol% ZnO; (c)7.5mol% In_2O_3; (d) 10mol% ZnO - 7.5 mol% In_2O_3

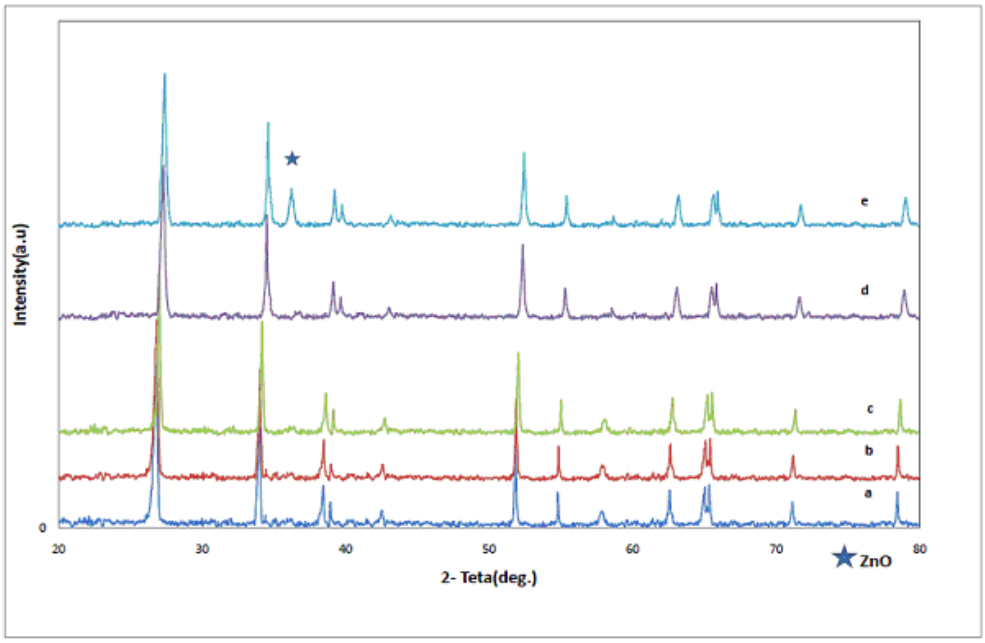

Fig. 2. XRD patterns of (a) pure SnO_2 and ZnO doped SnO_2 samples with (b) 1mol% , (c) 3mol% , (d) 5mol% and (e) 7mol%

smaller than Sn^{+4} (83 pm), it distorts the crystal structure of SnO_2 and decreases the lattice constants [1, 5]. At 7 mol% ZnO, the amount of ZnO is higher than solubility limit of SnO_2, and ZnO the peak appears as a second phase.

The XRD patterns of the samples with 10 and 12 mol% ZnO are shown in Fig. 3. ZnO peaks are seen in this figure and new phases (Zn_2SnO_4 and $ZnSnO_3$) are formed in the sample containing 12 mol% ZnO by sintering at 800°C.

Fig. 4 shows the XRD patterns of the pure SnO_2 and SnO_2 samples with 1 and 3 mol% of nano In_2O_3. In doped samples, a shift to left is seen in the diffraction peak positions. This behavior is similar to ZnO doping but in this case the ionic radius of In^{+2} (94nm) is higher

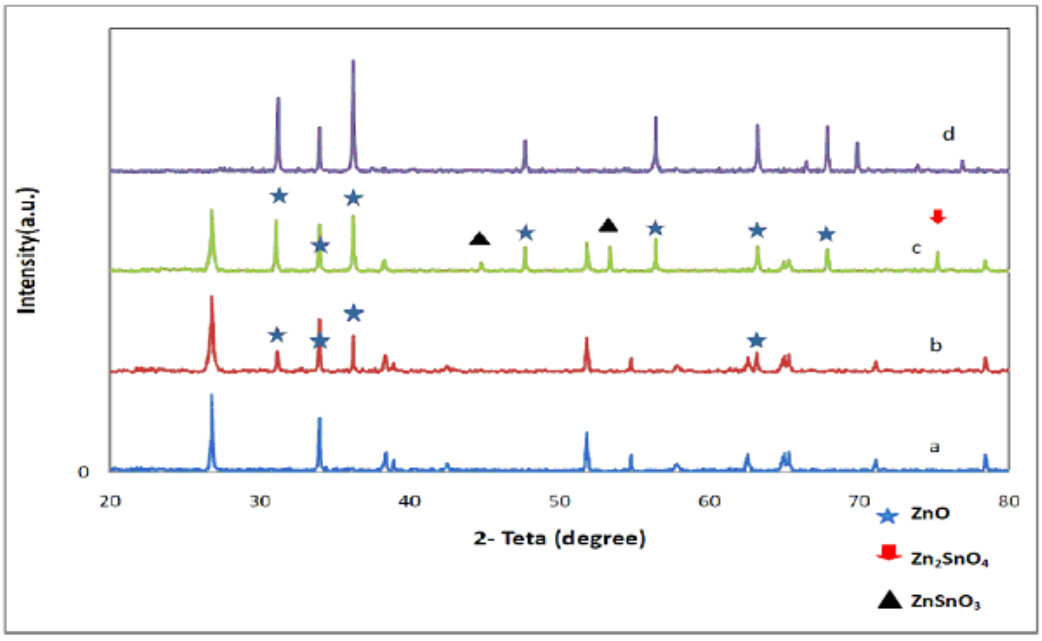

Fig. 3. XRD patterns of : (a) pure SnO_2 ; ZnO doped SnO_2 samples with (b) 10 mol% ; (c)12 mol% and (d) pure ZnO sample

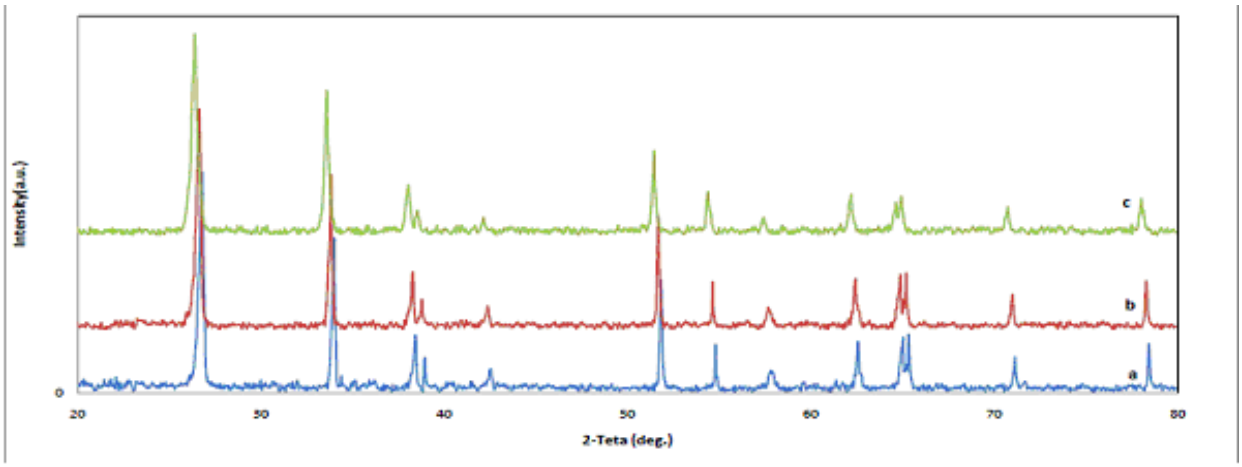

Fig. 4. XRD patterns of: (a) pure SnO_2 and SnO_2 samples with (b) 1 mol% and (c) 3 mol% In_2O_3

than that of Sn^{+4}, and lattice constants increase rather than decrease [3, 16].

The XRD patterns of the SnO_2 samples with 7.5 and 10mol % In_2O_3 are shown in Fig. 5. The solubility limit of In_2O_3 in SnO_2 was 3mol % and In_2O_3 peaks appeared in XRD patterns after this value. In_2SnO_5 was formed in the SnO_2 sample with 10 mol% In_2O_3.

The variation of the electrical resistivity of ZnO doped samples with time in 200ppm CO is shown in Fig. 6. In an ideal sensor, it must be maximum and this is seen in the sample containing 10 mol% ZnO. As expected, the addition of ZnO to SnO_2 up to 10 mol% increased the electrical resistivity and its variations. In the samples containing 11 and 12 mol% ZnO, the electrical resistivity was lower than its values in the 10 mol% ZnO doped sample. Improvement in the electrical resistivity of samples containing 1-7 mol% ZnO is due to Zn^{+2} substitution for Sn^{+4}, thereby increasing the oxygen vacancy concentration as can be seen in the following equation:

$$ZnO \overset{SnO_2}{\Longrightarrow} Zn_{Sn}^{''} + O_O^x + V_O^{\circ\circ} \qquad (1)$$

where the Kroger- Vink notations were used. Oxygen vacancies promote oxygen absorption and increase the thickness of depletion layers on the surface area of the sensor, resulting in a decrease in the carrier concentration and electron mobility. When the sensor is exposed to a reducing gas, it reacts with the absorbed

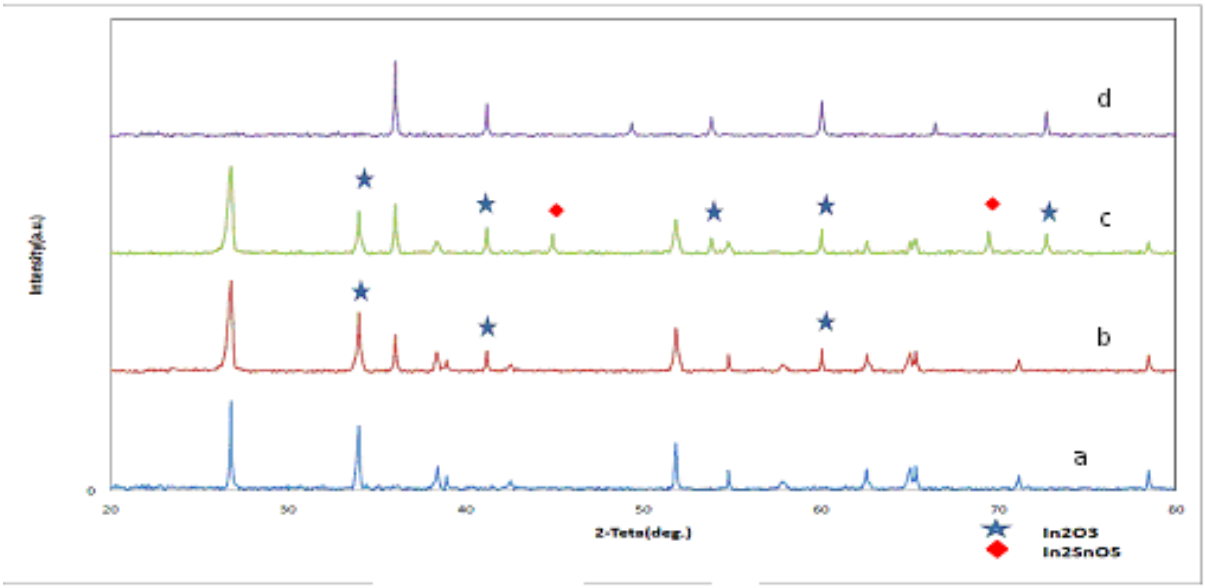

Fig. 5. XRD patterns of (a) Pure SnO_2 and In_2O_3 doped samples with (b) 7.5 mol% , (c) 10 mol% and (d) pure In_2O_3

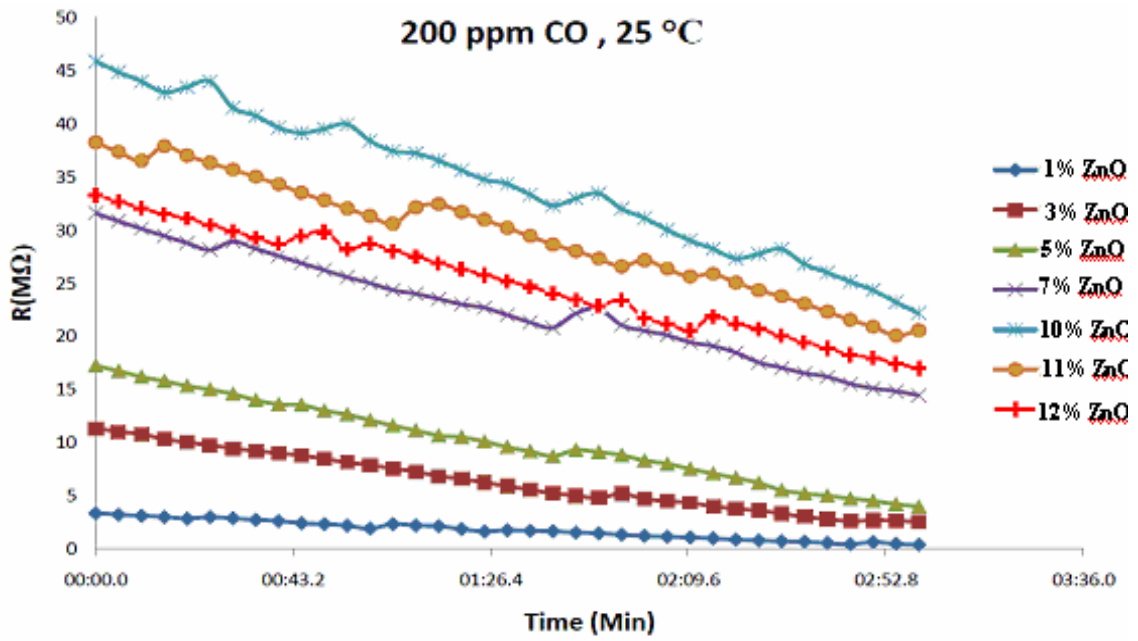

Fig. 6. Variation of electrical resistivity of ZnO doped SnO_2 samples with time in 200 ppm CO at 25°C

oxygens and releases the trapped electrons back to the conduction band, thereby increasing the carrier concentration and electron mobility of the sensor. Zinc can also react with oxygen species at the grain bounderies according to the following equations:

$$O_2 \rightarrow O_2^{x}{}_{(ads)} \qquad (2)$$

$$Zn''_{Sn} + O_2^{x}{}_{(ads)} \rightarrow Zn_{Sn}{}' + O_2{}'_{(ads)} \qquad (3)$$

$$Zn_{Sn}{}' + O_2{}'_{(ads)} \rightarrow Zn_{Sn}{}^{x} + 2O'_{(ads)} \qquad (4)$$

Therefore, the presence of Zn^{+2} in the SnO_2, enhances oxygen absorption and promotes the deplete layer formation, leading to an increase in the electrical resistivity and the reaction rate of CO with the sensor as the ZnO content of the sensor increases[12]. In the samples containing 7 and 10 mol% ZnO according to XRD results, the ZnO phase appears in the sensor as a second phase. Like SnO_2, ZnO is an n-type semiconductor and the formation of new interfaces between two phases (ZnO/SnO_2) will increase oxygen absorption and the consequently electrical resistivity. In the samples containing 11 and 12 mol% ZnO, the formation of the Zn_2SnO_4 phase, which is a non-semiconductor phase, decreases the sensor properties.

Fig. 7 shows the variation of electrical resistivity of nano In_2O_3 doped samples with time in 200ppm CO at 25°C. Like the ZnO effect, the addition of In_2O_3 to SnO_2 increases electrical resistivity. The enhancement in the electrical resistivity can be explained by the following equation:

$$In_2O_3 \xrightarrow{2SnO_2} 2In_{Sn}{}' + 3O_O{}^{x} + V_O{}^{\circ\circ} \qquad (5)$$

In^{3+} substitutes Sn^{+4} in the SnO_2 lattice, thereby increasing the oxygen vacancy concentration that increases the thickness of deplete layers [12]. Indium also reacts with

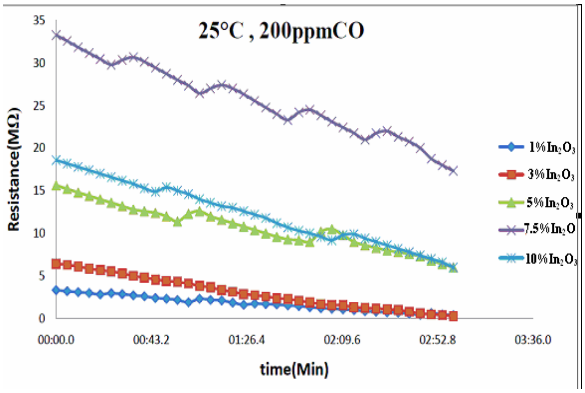

Fig. 7. Variation of electrical resistivity of nanoIn_2O_3 doped SnO_2 samples with time in 200 ppm

oxygen species and enhances oxygen absorption according to the following equations:

$$O_2 \rightarrow O_2^{x}{}_{(ads)} \quad (6)$$
$$In_{Sn}^{'} + O_2^{x}{}_{(ads)} \rightarrow In_{Sn}^{x} + O_2^{'}{}_{(ads)} \quad (7)$$
$$In_{Sn}^{'} + O_2^{'}{}_{(ads)} \rightarrow In_{Sn}^{x} + 2O^{'}{}_{(ads)} \quad (8)$$

In the samples containing 5 and 7.5 mol% In_2O_3, the In_2O_3 phase appears in the samples and like the ZnO phase, it increases the sensor activity. The formation of In_2SnO_5 in the samples containing 10mol% In_2O_3 decreases the sensor properties.

The effect of indium oxide on the electrical resistivity of SnO_2 is lower than that of zinc oxide. This is due to the charge valance of cations. Zn and In have valances +2 and +3, respectively. When Zn is doped to the SnO_2 lattice, two negative charges are added to the lattice, while In adds one negative charge to it. In the equations 3 and 4, each zinc cation reacts two times with oxygen but in the equations, 7 and 8 each indium cation has one reaction. Therefore, the effect of ZnO on the sensor properties is higher than that of In_2O_3.

The sensitivity (S) of the pure and doped SnO_2 samples with the maximum electrical resistance to 200ppm CO as a function of temperature is shown in Fig. 8. An ideal sensor has the maximum sensitivity at low temperatures [2, 3]. For the pure SnO_2 sample, the maximum sensitivity (4.2) occurs at 400°C. The maximum sensitivity (9.5) is seen in the sample containing 10 mol% ZnO and 7.5 mol% In_2O_3 at 200°C. The doped samples have the maximum sensitivity higher than the pure sample at lower temperatures. The addition of dopants like Zn or In to SnO_2 improves the deplete layer and when the amount of dopants exceeds the sensor solubility limit, the second phases with new heterogeneous interfaces (ZnO/SnO_2 or In_2O_3/SnO_2) are produced, enhancing the sensor sensitivity. In 10% ZnO-7.5% In_2O_3 doped sample the highest sensitivity is seen because of the presence of two types of dopant with the optimum values and three phases. The sensitivity of 10% ZnO doped sample is better than 7.5% In_2O_3 doped sample due to higher activity of Zinc relative to Indium.

It is known that the performance of sensors is dependent on response and recovery times [18]. Fig.9 shows the response and recovery times of doped SnO_2 samples which are exposed to 200 ppm CO at 25°C. The minimum response and recovery times are for 10% ZnO-7.5% In_2O_3 doped sample, which are about 10 and 9 min, respectively.

4. Conclusions

The nano ZnO and In_2O_3 additives improved the sensor properties of SnO_2. The electrical resistivity and sensitivity increased and the maximum sensitivity temperature, as well as response and recovery times decreased. Additives had a slight effect on the microstructure. The optimum values for additives were 10 and 7.5 mol% for ZnO and In_2O_3, respectively. ZnO was more effective than In_2O_3 on the sensing properties. The

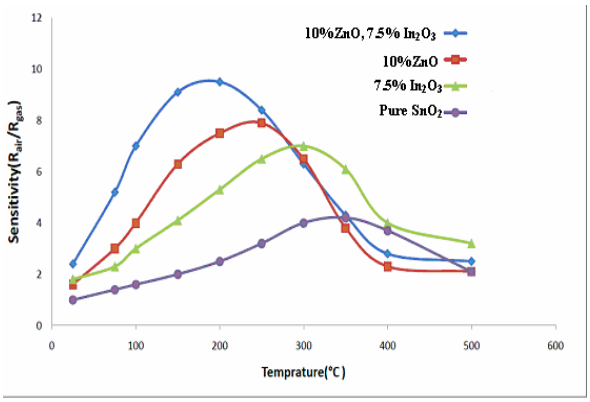

Fig. 8. The temperature dependence of the sensitivity of SnO_2 and ZnO/ In_2O_3 doped SnO_2 to 200-ppm CO gas

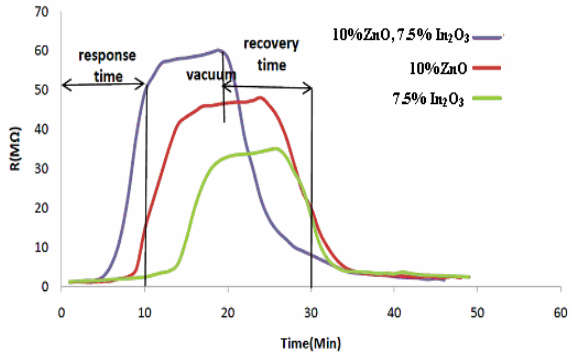

Fig. 9. Response and recovery time for ZnO and In_2O_3 added samples.

optimum sensing properties were obtained in the sample containing 10 mol% ZnO and 7.5 mol% In_2O_3.

References

1. Moulson, J., Herbert, J.M., (2003) Electroceramics John Wiley & Sons, Inc.
2. Ramgir, N.S., Hwang, Y.K., Jhung, S.H., Mulla, I.S., Chang, *J.S., Sens. Actuators B*, Vol. 114 (2006) pp. 275–282.
3. Zhanga, T., Liu, L., Qi, Q., Li, Sh., Lu, G., *Sens. Actuators B*, Vol. 139 (2009) pp. 287–291.
4. Bahrami, B., Khodadadi, A., Kazemeini, M., Mortazavi, Y., *Sens. Actuators B*, Vol. 133 (2008) pp. 352–356.
5. Yu, J.H., Choi, G.M., *Sens. Actuators B*, Vol. 52 (1998) pp. 251-256.
6. Moon, W.J., Yu, J.H., Choi, G.M., *Sens. Actuators B*, Vol. 75 (2001) pp. 56-61.
7. Moon, W.J., Yu, J.H., Choi, G.M., *Sens. Actuators B*, Vol. 87 (2002) pp. 464-470.
8. Ozaki, Y., Suzuki, S., Morimitsu, M., Matsunaga, M., *Sens. Actuators B*, Vol. 62 (2000) pp. 220–225.
9. Lee, J.H., *Sens. Actuators B*, Vol. 140 (2009) pp. 319-336.
10. Cerd Belmonte, J., Manzano, J., Arbiol, J., Cirera , A., Puigcorbe , J., Vila , A., Sabate, N., Gracia , I., Cane , C., Morante, J.R., *Sens. Actuators B*, Vol. 114 (2006) pp. 881-892.
11. Choe, Y.S., *Sens. Actuators B*, Vol. 77 (2001) pp. 200-208.
12. Habibzadeh, S., Khodadadi, A. A., Mortazavi , Y., *Sens. Actuators B*, Vol. 144 (2010) pp. 131–138
13. Korotcenkov, G., Cho, B.K., *Sen. Actuators B*, Vol. 142 (2009) pp. 321–330.
14. M. Suzuki, M. Muraoka, Y. Sawada , J. Matsushit, *Materials Science and Engineering B*, Vol. 54 (1998) pp. 46–50.
15. Zeng, Y., Dongliang , J., Masuda, Y., Dewei , Ch., *Sens. Actuators B*, Vol. 137 (2009) pp. 630–636.
16. Lina, Ch., Yuan Fangb, Y., Wann Linb, Ch., Tunneyd, J.J., Chuan Ho, K., *Sens. Actuators B*, Vol. 146 (2010) pp. 28–34.
17. Choi, U.S., Sakai, G., Shimanoe, K., Yamazoe, N., *Sens. Actuators B*, Vol. 107 (2005) pp. 397–401.
18. M. Vilaseca, J. Coronas, A. Cirera, A. Cornet, J.R. Morante, J. Santamaria, *Sens. Actuators B*, Vol. 133 (2008) pp. 435–441.